



OPEN

SUBJECT AREAS:

ELECTRICAL AND  
ELECTRONIC  
ENGINEERINGSOLAR ENERGY AND  
PHOTOVOLTAIC  
TECHNOLOGY

Received

13 August 2014

Accepted

5 November 2014

Published

21 November 2014

Correspondence and requests for materials should be addressed to D.-K.L. (dklee@kist.re.kr); S.H. (shhan@kist.re.kr) or J.Y. (yj@skku.ac.kr)

\* These authors contributed equally to this work.

# Triple-Junction Hybrid Tandem Solar Cells with Amorphous Silicon and Polymer-Fullerene Blends

Taehee Kim<sup>1\*</sup>, Hyeok Kim<sup>1\*</sup>, Jinjoo Park<sup>2\*</sup>, Hyungchae Kim<sup>3,4</sup>, Youngwoon Yoon<sup>1</sup>, Sung-Min Kim<sup>1</sup>, Chonghoon Shin<sup>2</sup>, Heesuk Jung<sup>1</sup>, Inho Kim<sup>5</sup>, Doo Seok Jeong<sup>5</sup>, Honggon Kim<sup>1</sup>, Jin Young Kim<sup>1</sup>, BongSoo Kim<sup>1</sup>, Min Jae Ko<sup>1</sup>, Hae Jung Son<sup>1</sup>, Changsoon Kim<sup>3,4</sup>, Junsin Yi<sup>2</sup>, Seunghee Han<sup>1</sup> & Doh-Kwon Lee<sup>1</sup>

<sup>1</sup>Photo-electronic Hybrids Research Center, Korea Institute of Science and Technology (KIST), Seoul 136-791, Korea, <sup>2</sup>College of Information and Communication Engineering, Sungkyunkwan University, Suwon 440-746, Korea, <sup>3</sup>Department of Nano Science and Technology, Graduate School of Convergence Science and Technology, Seoul National University, Seoul 151-747, Korea, <sup>4</sup>Advanced Institutes of Convergence Technology, Suwon, Gyeonggi 443-270, Korea, <sup>5</sup>Electronic Materials Research Center, Korea Institute of Science and Technology (KIST), Seoul 136-791, Korea.

Organic-inorganic hybrid tandem solar cells attract a considerable amount of attention due to their potential for realizing high efficiency photovoltaic devices at a low cost. Here, highly efficient triple-junction (TJ) hybrid tandem solar cells consisting of a double-junction (DJ) amorphous silicon (a-Si) cell and an organic photovoltaic (OPV) rear cell were developed. In order to design the TJ device in a logical manner, a simulation was carried out based on optical absorption and internal quantum efficiency. In the TJ architecture, the high-energy photons were utilized in a more efficient way than in the previously reported a-Si/OPV DJ devices, leading to a significant improvement in the overall efficiency by means of a voltage gain. The interface engineering such as tin-doped In<sub>2</sub>O<sub>3</sub> deposition as an interlayer and its UV-ozone treatment resulted in the further improvement in the performance of the TJ solar cells. As a result, a power conversion efficiency of 7.81% was achieved with an open-circuit voltage of 2.35 V. The wavelength-resolved absorption profile provides deeper insight into the detailed optical response of the TJ hybrid solar cells.

There have been many challenging studies of thin-film solar cells as part of the effort to advance renewable energy technologies<sup>1–3</sup>. The main objectives of the research on next-generation photovoltaic (PV) cells, as alternatives to the currently available crystalline silicon PV systems, are to realize low-cost production as well as to enhance the power conversion efficiency (PCE). The tandem cell architecture, in which multiple solar cells with different bandgaps are stacked in series, is a promising strategy to alleviate the innate energy losses of single-junction (SJ) solar cells, i.e., the thermalization loss of high-energy photons and the transmission loss of low-energy photons<sup>4–9</sup>. In particular, hybrid tandem solar cells consisting of amorphous inorganic semiconductors and solution-processible organic active materials are attractive candidates due to their low material costs, simple manufacturing processes, and tunable optoelectric properties. Previously, we reported organic-inorganic hybrid tandem solar cells which were realized by combining an amorphous silicon (a-Si) front cell and an organic photovoltaic (OPV) rear cell with a low-bandgap semiconducting polymer<sup>10,11</sup>. These cells were capable of utilizing broad-spectrum solar light. However, to reach a current-matched condition, the thickness of the a-Si front cell was limited so as to secure the optical absorption of the OPV rear cell in the double-junction (DJ) solar cells<sup>11,12</sup>. Consequently, the high-energy photons were not fully utilized by the thin a-Si front cell.

Herein, we present a triple-junction (TJ) hybrid tandem solar cell with two a-Si subcells and an OPV rear cell in which the high-energy photons can be sufficiently harnessed, thus contributing to the improvement in the overall PCE by means of a voltage gain. In order to maximize the PCE of TJ hybrid tandem solar cells, the solar spectrum should be evenly utilized by the three subcells, fulfilling the current-matching requirement. However, determining the mutual influence of the optical and electrical performance of individual subcells in a series-connected tandem configuration is complicated. Thus, a rational design of such multi-junction tandem devices is of great importance to alleviate the tedious and repetitive experiments for the device optimization. In order to design the TJ device in a logical manner, we carried out an optical simulation based on the Transfer Matrix (TM) formalism<sup>13</sup>

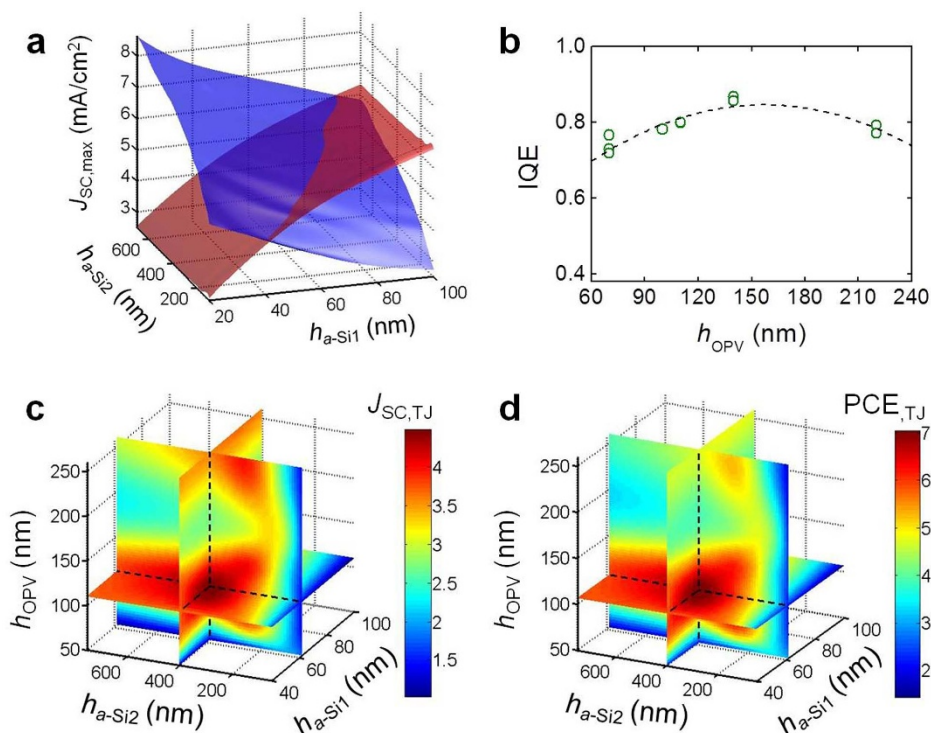


**Figure 1 | Simulation to optimize the TJ hybrid tandem solar cell.** (a) 3-D plot of current-generating capacities of the a-Si front (a-Si<sub>1</sub>) and rear (a-Si<sub>2</sub>) cells in the DJ configuration versus their *i*-layer thicknesses. (b) IQE of single-junction OPV solar cells as a function of active layer thickness. The dashed line is a quadric fit with polynomial regression. 4-D plot of calculated  $J_{SC}$  (c) and PCE (d) of the TJ hybrid tandem cell (predicted optimal thicknesses:  $h_{a-Si1} = 62$  nm,  $h_{a-Si2} = 400$  nm,  $h_{OPV} = 107$  nm).

combined with empirical data pertaining to the electrical properties. The TJ hybrid tandem solar cell optimized on the basis of the simulation results exhibited a PCE of 7.81% with an open-circuit voltage ( $V_{OC}$ ) of 2.35 V.

## Results

To perform a simulation of the TJ tandem devices in this study, we elaborated Gilot's method<sup>5</sup> which is based on optical absorption and internal quantum efficiency (IQE). We calculated the optical absorption of the individual subcells using the Transfer Matrix (TM) formalism<sup>13</sup> from refractive indices ( $n$ ) and extinction coefficients ( $k$ ) measured with ellipsometry (Fig. S1a). For the OPV subcell, we used poly{4,8-*bis*[(2-ethylhexyl)oxy]benzo[1,2-*b*:4,5-*b'*]dithiophene-2,6-diyl-alt-3-fluoro-2-[(2-ethylhexyl)carbonyl]thieno[3,4-*b*]thiophene-4,6-diyl} (PTB7) (Fig. S1b) as an electron-donating conjugated polymer and (6,6)-phenyl C<sub>61</sub> butyric acid methyl ester (PC<sub>61</sub>BM) as an electron acceptor. First, a simulation was carried out with an a-Si DJ tandem cell to determine the optimal thicknesses of the subcells. By calculating the number of photons absorbed by two a-Si cells stacked in series (Fig. S2), the short-circuit current density ( $J_{SC}$ ) of each cell was calculated according to

$$J_{SC} = q \int \Phi \cdot Abs \cdot IQE \cdot d\lambda, \quad (1)$$

where  $q$ ,  $\Phi$ ,  $Abs$ , and  $IQE$  are the elementary charge, the photon flux of the standard air mass (AM) 1.5G solar spectrum, the ratio of the number of absorbed photons in the active layer to the number of incident photons, and the ratio of the number of carriers collected at an electrode to the number of photons absorbed in the active layer, respectively<sup>14</sup>. For simplicity, an IQE of unity was used in equation (1) to yield maximal values of  $J_{SC}$  (namely  $J_{SC,max}$ ) without sacrificing the legitimacy of the argument. Fig. 1a shows the calculated  $J_{SC,max}$  of a-Si front (red surface) and rear cells (blue surface) versus

their intrinsic layer (*i*-layer) thicknesses in a-Si DJ tandem cells. According to the Kirchhoff's law, the  $J_{SC}$  value of a series-connected tandem cell is determined by the lowest value of the subcells. Accordingly, the  $J_{SC,max}$  values of the a-Si DJ tandem cell and corresponding thicknesses of the subcells were evaluated as depicted by the cross-section of the two surfaces shown in Fig. 1a.

The above simulation was extended to a TJ tandem cell consisting of an a-Si DJ cell and an OPV rear cell. For this calculation, we extracted the wavelength ( $\lambda$ )-independent (or solar-spectrum-weighted) IQE ( $IQE_{\Phi}$ ) of the OPV cells from the ratio of  $J_{SC}$  (obtained from measured external quantum efficiency (EQE) data) to  $J_{SC,max}$  (calculated from optical absorption assuming that the IQE is unity) as

$$IQE_{\Phi} = \frac{J_{SC}}{J_{SC,max}} = \frac{q \int \Phi \cdot EQE \cdot d\lambda}{q \int \Phi \cdot Abs \cdot I \cdot d\lambda}. \quad (2)$$

Fig. 1b shows the calculated  $IQE_{\Phi}$  of OPV single cells estimated with equation (2) as a function of the active layer thickness. For a-Si cells, the IQE was assumed to have a more realistic value of 0.95<sup>15,16</sup>. The  $J_{SC}$  values of the subcells in the TJ tandem architecture were then calculated according to equation (1) with varying thicknesses of the active layer, and therefrom the  $J_{SC}$  values of the TJ tandem cells were assessed according to the Kirchhoff's law. Simulation results for the optimization of the active layer thicknesses of the TJ hybrid tandem solar cell are shown in Fig. 1c and 1d. For a clear presentation of the result with four parameters in Fig. 1c, i.e., the active layer thicknesses of the front a-Si cells, the middle a-Si cells, the rear OPV cells, and the  $J_{SC}$  values of TJ cells ( $h_{a-Si1}$ ,  $h_{a-Si2}$ ,  $h_{OPV}$ , and  $J_{SC,TJ}$ ), a four-dimensional cross-section plot was employed (see also Fig. S3). Subsequently, the PCE of the TJ tandem cell was assessed using this  $J_{SC}$  according to the definition of  $PCE = J_{SC} V_{OC} FF / P_0$ , where  $V_{OC}$ ,  $FF$ , and  $P_0$  are the open-circuit voltage, fill factor, and input power, respectively. For this calculation, the  $FF$  and  $V_{OC}$  values of the OPV

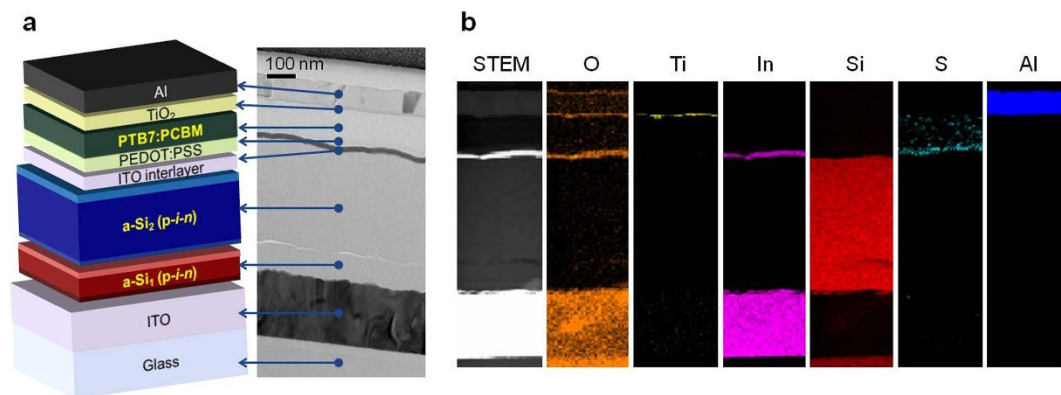


**Figure 2** | Cross-sectional TEM analysis. (a) A schematic showing the device configuration of the TJ hybrid tandem solar cell and the corresponding cross-sectional TEM image. (b) STEM-EDX element mapping.

cells were measured as a function of the active layer thickness (see Fig. S4). The FF and  $V_{OC}$  of the a-Si cells are assumed to be constant. First, the  $V_{OC}$  of the TJ tandem cell was estimated at the sum of the  $V_{OC}$  values of the subcells. The FF value of the TJ tandem cell was estimated to be the median value between those of the a-Si DJ and OPV cells. The PCE values of the TJ hybrid tandem solar cells estimated in this way are presented in Fig. 1d. The result shows that the optimum active layer thicknesses are 62 nm, 400 nm, and 107 nm for  $h_{a-Si1}$ ,  $h_{a-Si2}$ , and  $h_{OPV}$ , respectively. In this calculation, the simplification that the IQE, FF, and  $V_{OC}$  of the a-Si cells are independent of their  $i$ -layer thicknesses may give rise to a slight overestimation of the optimum thickness of the middle a-Si cell because, in reality, these parameters tend to decrease with the  $i$ -layer thickness of a-Si cells due to the inefficient charge collection and consequent recombination<sup>17,18</sup>. Taking these tendencies into account, it can be inferred that a slightly thinner  $i$ -layer of the middle a-Si cell may be preferable to minimize an efficiency loss.

Based on the simulation results, we fabricated TJ hybrid tandem cells with the optimized active layer thicknesses, as shown in Fig. 2. The absorber-layer thicknesses of the fabricated TJ cell were 70 nm, 350 nm, and 110 nm for  $h_{a-Si1}$ ,  $h_{a-Si2}$ , and  $h_{OPV}$ , respectively, as confirmed by the cross-sectional TEM image shown in Fig. 2a. An elemental mapping analysis with energy-dispersive X-ray (EDX) spectroscopy (Fig. 2b) verifies the homogeneously deposited multiple layers including a-Si, tin-doped In<sub>2</sub>O<sub>3</sub> (ITO), poly(3,4-ethylenedioxythiophene):poly(styrene sulfonate) (PEDOT:PSS), TiO<sub>2</sub>, and Al layers, ensuring the uniform electric fields in the active layers, a condition which is essential for efficient charge collection.

Fig. 3a shows the  $J-V$  characteristics of the solar cells under AM1.5G illumination. The corresponding photovoltaic parameters are listed in Table 1. To reduce any detrimental interfacial resistance due to the incompatibility between the a-Si and the PEDOT:PSS

layers, a thin ITO interlayer (ITL) was introduced by DC magnetron sputtering<sup>11</sup>. It was noted that, by inserting the ITO ITL, a kink in the vicinity of the  $V_{OC}$  in the  $J-V$  curve for the TJ cell was eliminated, which significantly augmented the FF value. Furthermore, to enhance the wettability of the PEDOT:PSS solution onto the ITO interlayer surface, we applied a short (5 s) UV-ozone (UVO) treatment before depositing the PEDOT:PSS layer, which turned out to enhance the photovoltaic performance of the resulting devices. As a result, a PCE of 7.81% was achieved with a  $J_{SC}$  of 5.13 mA cm<sup>-2</sup>, a  $V_{OC}$  of 2.35 V, and a FF of 0.649 for the TJ hybrid tandem solar cell. These PCE and  $V_{OC}$  values are the highest among organic-inorganic hybrid tandem solar cells reported to date<sup>12</sup>. The EQEs of the subcells in the TJ tandem solar cell were measured under a highly unbalanced photocurrent condition using additional light sources with controlled wavelengths, as depicted in Fig. 3b. It is shown that the photons with wavelengths of 300 to 520 nm were absorbed by the front a-Si cell, the photons at 520–630 nm were utilized by the middle a-Si cell, and the OPV rear cell harnessed the photons in the wavelength range of 620–800 nm, respectively. One may recognize that the EQE of the OPV rear cell is enhanced substantially as compared to that of the single-junction rear cell (Fig. S1c). The origin of this result should be associated with the difference in the adjacent layers of OPV, i.e., the transparent ITO glass in the SJ OPV device (Fig. S1d) and the reflective a-Si<sub>2</sub> layer in the TJ device (Fig. 2).

To better understand how light can be utilized efficiently by the TJ tandem device, we calculated the fractional spectral distribution using the TM method as shown in Fig. 4a, including the absorption and reflection of all the layers with their corresponding thicknesses to those in Fig. 2. The absorption fractions by inactive  $p$ -type and  $n$ -type Si layers which cannot contribute to the generation of photocurrent are marked with dashed lines. As shown in Fig. 4a, the fractional absorption of the front a-Si cell appeared to be larger than that of the

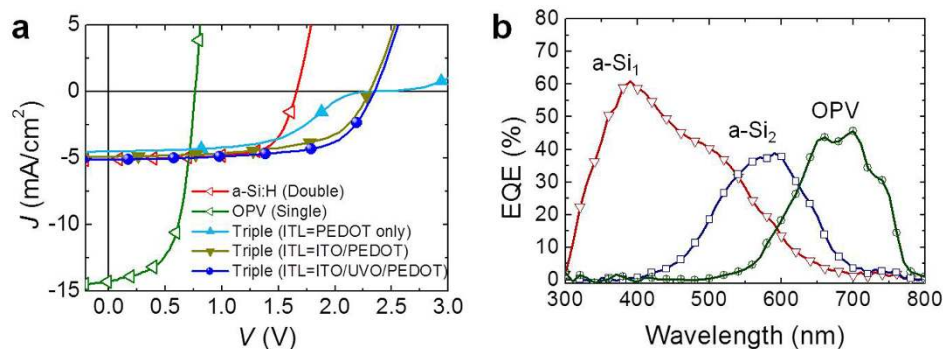


**Figure 3** | Photovoltaic performance and spectral response of the TJ tandem cell with active layer thicknesses of 70 nm, 350 nm, and 110 nm for the front, middle, and rear cell, respectively. (a) Illuminated  $J-V$  characteristics and (b) measured EQEs.





Table 1 | Device parameters of single-junction OPV, double-junction a-Si, and triple-junction hybrid solar cells

Device		$J_{sc}$ (mA cm <sup>-2</sup> )	$V_{oc}$ (V)	FF	PCE (%)
Single-junction	OPV	14.27	0.76	0.589	6.41
Double-junction	a-Si	5.10	1.66	0.697	5.89
Triple-junction	PEDOT only	4.50	2.33	0.507	5.32
	ITO ITL/PEDOT	4.91	2.31	0.601	6.80
	ITO ITL/UVO/PEDOT	5.13	2.35	0.649	7.81

middle a-Si cell. It should be noted, however, that this spectral distribution shows only the optical properties of each layer. Considering the possible electrical loss in the thicker middle cell as mentioned previously, the experimentally determined optimal thicknesses are regarded as a consequence of the compromise between the optical and electrical performances. Fig. 4b shows the EQEs calculated from the optical absorption profiles, which are in good agreement with the measured EQE (Fig. 3b), thus validating the simulation methodology employed in this work.

## Discussion

In order to gain more insight into the detailed optical response of the TJ hybrid tandem device, we calculated the spatially resolved optical absorption profiles at the optimized thickness, as shown in Fig. 5. The photon absorption rate  $G(x)$  was derived from the time-averaged energy density dissipated per unit volume per second,  $Q(x)$ , in layer  $j$  at position  $x$  as

$$G_j(x) = \frac{\lambda}{hc} \cdot \frac{Q_j(x)}{I_0}, \text{ where } Q_j(x) = \frac{1}{2} c \cdot \epsilon_0 \cdot \alpha_j \cdot n_j |E_j(x)|^2. \quad (3)$$

Here,  $h$ ,  $c$ ,  $\epsilon_0$ ,  $\alpha$ , and  $E(x)$  are the Planck constant, the speed of light, the permittivity of free space, the absorption coefficient ( $\alpha = 4\pi k/\lambda$ ), and the field of electromagnetic wave, respectively.  $I_0$  is the energy density per unit area of the incident electric field ( $I_0 = c\epsilon_0 n E_0^2/2$ ), where  $E_0$  is the incident electric field. Fig. 5a and b shows the integral of the normalized light intensity ( $=\int |E(x)|^2/E_0^2 d\lambda$ ) and the absorbed photon flux ( $=\int \Phi G(x) d\lambda$ ). It is important to note that photon absorption at the OPV active layer is enhanced in the tandem configuration as compared to the single-junction OPV rear cell. This enhanced absorption is consistent with the measured EQE (Fig. 3b in comparison with Fig. S1c), which can be attributed to the resonant absorption between the reflective a-Si<sub>2</sub> and Al surfaces<sup>19</sup>. We also present a wavelength-resolved profile of the absorbed photon flux  $\Phi G(x)$  in Fig. 5c, which shows efficient photon absorption at a short wavelength by a-Si<sub>1</sub> and at a long wavelength by OPV subcells. In Fig. 5b, a sharp absorption profile can be observed at the thin  $i$ -layer of the front a-Si subcell; this is attributed to its high extinction coefficient at wavelengths from 300 nm to 550 nm (Fig. S1a). The middle

a-Si<sub>2</sub> subcell absorbs the photons at wavelengths from 480 nm to 650 nm that pass by the thin a-Si<sub>1</sub> subcell, as visualized in Fig. 5c. As the a-Si layer has a low  $k$  in this wavelength regime (Fig. S1a), the thickness of the middle a-Si<sub>2</sub> subcell should be thick enough to ensure sufficient absorption. Eventually, the photons at long wavelengths from 620 nm to 770 nm are mainly absorbed by the rear OPV subcell (Fig. 5c) to reach the current-matching condition.

In summary, we presented highly efficient TJ hybrid tandem solar cells with amorphous silicon (a-Si) and PTB7:PCBM blends. The PCE was significantly enhanced as compared to DJ solar cells<sup>11,12</sup> by utilizing the solar spectrum in a more efficient way, leading to a high voltage gain. In order to optimize the TJ device in a logical manner, we performed a simulation based on optical absorption and the IQE. Our simulation results provide valuable insight into the fabrication of efficient tandem solar cells. The optimized TJ hybrid tandem solar cell showed a PCE of 7.81% and a  $V_{oc}$  of 2.35 V. According to our simulation results (Fig. S5 and S6) based on the same method described in the previous section, further improvements (up to ~12%) can be achieved by realizing non-overlapping spectral responses via bandgap tuning of the subcells.

## Methods

**Simulation.** The calculation of optical absorption was performed with the transfer matrix (TM) method. The code is written in Matlab (The MathWorks, Inc.), a mathematical software package based on matrix manipulations. The optical constants used in the calculations were measured with a variable angle ellipsometer (VASE, Woollam).

**Single-junction OPV cells.** PTB7 and PCBM were purchased from 1-material (Quebec, Canada) and Nano-C, Inc. (MA, USA), respectively. Single-junction PTB7:PCBM PV devices were fabricated on pre-patterned tin-doped In<sub>2</sub>O<sub>3</sub> (ITO) substrates (15 Ω/square, Samsung Corning). The ITO substrate was cleaned by sonication in acetone and isopropyl alcohol, sequentially. After drying at 80°C for 30 min with a subsequent UV-ozone treatment for 20 min, poly(3,4-ethylenedioxythiophene):poly(styrene sulfonate) (PEDOT:PSS) (Clevis P, VP AI 4083) as a hole-transporting layer was deposited onto the ITO substrate by spin-coating from an aqueous solution in air. The PEDOT:PSS layer was dried at 110°C for 10 min. In a nitrogen-filled glove box, the PTB7:PCBM photoactive layer was deposited onto the dried PEDOT:PSS layer by spin-coating from a chlorobenzene solution containing 3 vol% 1-diiodooctane with a PTB7:PCBM weight ratio of 1:1.25 and a PTB7 concentration of 10 mg ml<sup>-1</sup>. After drying at 70°C for 5 min and in a vacuum for 10 min, a TiO<sub>2</sub> electron-transporting layer was deposited onto the

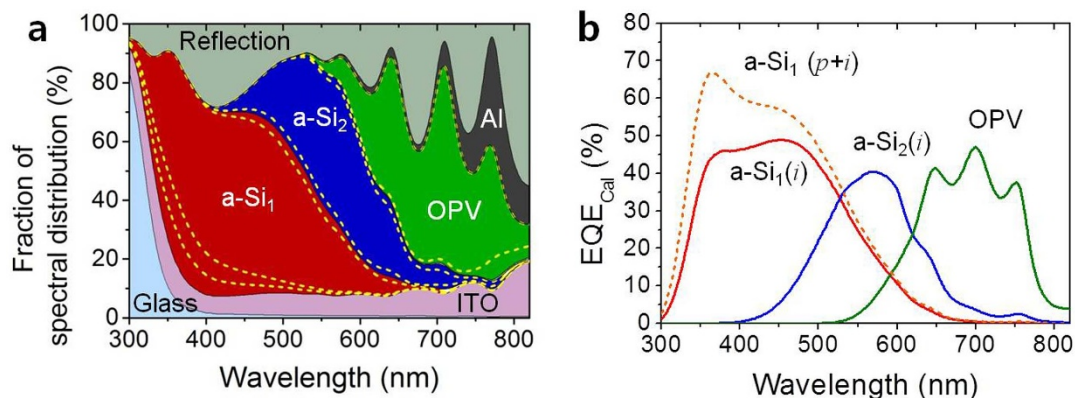
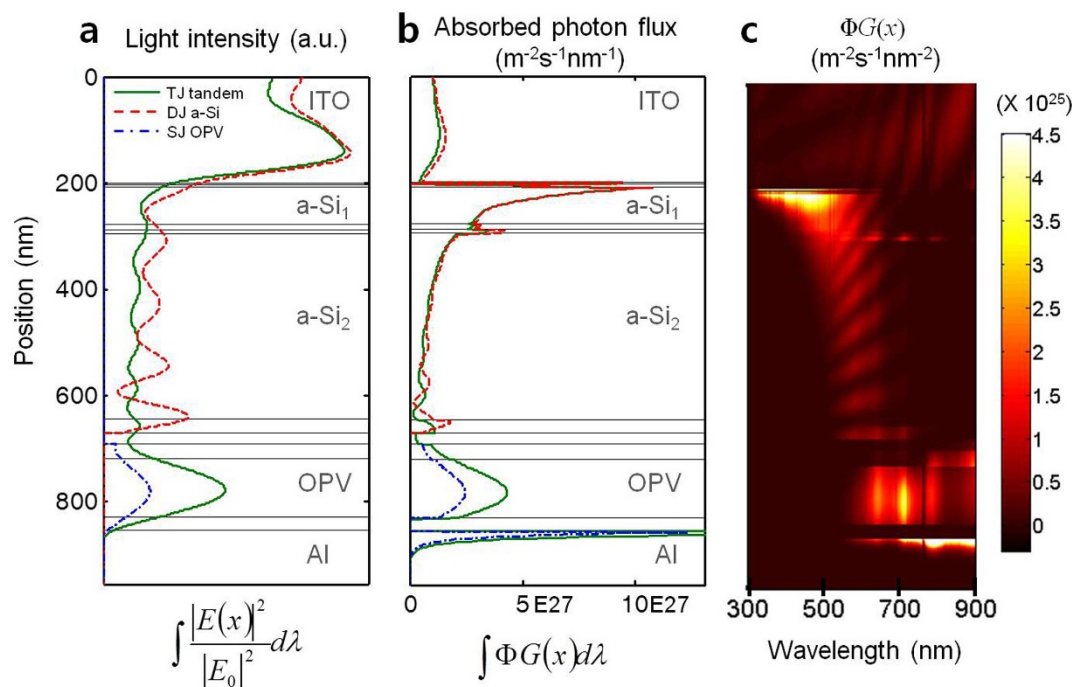


Figure 4 | Simulated spectral response of TJ tandem cell with active layer thicknesses of 70 nm, 350 nm, and 110 nm. (a) Fractional spectral distribution and (b) absorption profiles as functions of wavelength. Dashed lines in (a) and (b) indicate interfacial layers at their adjacent active layers.



**Figure 5 | Absorption profiles in the TJ tandem devices as a function of spatial position.** (a) Normalized light intensity, (b) absorbed photon flux profiles, and (c) wavelength-resolved profile of absorbed photon flux.

active layer by spin-coating using ethanol dispersion of TiO<sub>2</sub> nanoparticles (0.4 wt%) at 4000 rpm. An Al electrode was deposited by thermal evaporation at  $\sim 3 \times 10^{-6}$  Torr. The active area of the solar cells (0.20 cm<sup>2</sup>) was determined by the overlapped area between the ITO and the Al electrodes.

**Double-junction a-Si solar cells.** The a-Si layers with the *p/i/n* sequence for the DJ solar cells have film thicknesses of 88 nm (8 nm/70 nm/10 nm for *p/i/n*) and 382 nm (7 nm/350 nm/25 nm for *p/i/n*) for the front and middle cell, respectively. The a-Si layers were deposited onto the ITO substrate by means of a plasma-enhanced chemical vapor deposition (PE-CVD) system. The detailed deposition condition of the PE-CVD process is described in the Supporting Information.

**Triple-junction hybrid tandem solar cells.** A 20-nm-thick ITO interconnecting layer was deposited onto the n-type a-Si layer by DC magnetron sputtering at a film growth rate of 0.1 nm s<sup>-1</sup> using an ITO target (10 wt% of SnO<sub>2</sub>, 99.99% purity) with an operating pressure of 3 mTorr, an Ar gas flow rate of 6 sccm, and an RF power of 50 W. The conductive ITO interconnecting layer was confined to the active area by a shadow mask to prevent a short circuit. The surface of the as-deposited ITO interlayer was UV-ozone treated for 5 s before depositing the PEDOT:PSS layer. The TJ hybrid tandem solar cells were fabricated by depositing the PEDOT:PSS, PTB7:PCBM, TiO<sub>2</sub> layers and the Al electrode sequentially as mentioned above.

**Characterization.** The current density–voltage (*J–V*) characteristics were measured by a Keithley 2400 source meter with a 150 W solar simulator (Yamashita Denso Corp., YSS-50A) under a light intensity of 100 mW cm<sup>-2</sup> (1 sun, AM 1.5G illumination). The cross-sectional structure and the atomic distribution were investigated by TEM (FEI, Tecnai F20G2) equipped with STEM-EDX. The cross-sectional TEM sample was prepared by means of focused ion beam (FEI Nova 600 NanoLab) milling. The external quantum efficiency (EQE) was measured using an incident photo-to-current efficiency (IPCE) measurement system G1218a (PV measurements, Inc., Boulder, USA). To extract the EQE selectively from each individual subcell in the tandem device, we used two white light emitting diodes (LED) with optical cut-off filters (Andover Corporation, Salem, USA). The light intensity of a white LED was about 15 mW cm<sup>-2</sup> (0.15 sun). The EQE signal of series-connected triple-junction tandem cells corresponds to that of the current-limiting subcell. Thus, we rendered the front a-Si subcell current-limiting by using a 550-nm-high-pass optical filter along with the white LED (bias light with  $\lambda > 550$  nm). The middle a-Si subcell was made current-limiting by employing two light sources and two optical filters (500-nm-low-pass and 650-nm-high-pass) to apply light bias ( $\lambda_1 < 500$  nm and  $\lambda_2 > 650$  nm) to the front a-Si and the rear OPV subcells. Likewise, the rear OPV cell was taken as the limiting cell by using a 600-nm-low-pass filter with one white LED ( $\lambda < 600$  nm).

- Todorov, T. K. *et al.* Beyond 11% efficiency: Characteristics of state-of-the-art Cu<sub>2</sub>ZnSn(S,Se)<sub>4</sub> solar cells. *Adv. Energy Mater.* **3**, 34–38 (2013).
- He, Z. *et al.* Enhanced power-conversion efficiency in polymer solar cells using an inverted device structure. *Nat. Photon.* **6**, 591–595 (2012).
- Ameri, T., Dennler, G., Lungenschmied, C. & Brabec, C. J. Organic tandem solar cells: A review. *Energy Environ. Sci.* **2**, 347–363 (2009).
- Gilot, J., Wienk, M. & Janssen, R. Optimizing polymer tandem solar cells. *Adv. Mater.* **22**, E67–E71 (2010).
- Wang, X. *et al.* Tandem colloidal quantum dot solar cells employing a graded recombination layer. *Nat. Photon.* **5**, 480–484 (2011).
- Beiley, Z. M. & McGehee, M. D. Modeling low cost hybrid tandem photovoltaics with the potential for efficiencies exceeding 20%. *Energy Environ. Sci.* **5**, 9173–9179 (2012).
- You, J. *et al.* A polymer tandem solar cell with 10.6% power conversion efficiency. *Nat. Commun.* **4**, 1446–1455 (2013).
- Kim, S. *et al.* Remarkable progress in thin-film silicon solar cells using high-efficiency triple-junction technology. *Sol. Energy Mater. Sol. Cells* **119**, 26–35 (2013).
- Kim, T. *et al.* Organic-inorganic hybrid tandem multijunction photovoltaics with extended spectral response. *Appl. Phys. Lett.* **98**, 183503-1–183503-3 (2011).
- Kim, T. *et al.* Hybrid tandem photovoltaic devices with a transparent conductive interconnecting recombination layer. *Mater. Res. Bull.* **47**, 3040–3043 (2012).
- Seo, J. H. *et al.* High efficiency inorganic/organic hybrid tandem solar cells. *Adv. Mater.* **24**, 4523–4527 (2012).
- Pettersson, L. A., Roman, L. S. & Inganäs, O. Modeling photocurrent action spectra of photovoltaic devices based on organic thin films. *J. Appl. Phys.* **86**, 487–496 (1999).
- Peumans, P., Yakimov, A. & Forrest, S. R. Small molecular weight organic thin-film photodetectors and solar cells. *J. Appl. Phys.* **93**, 3693–3723 (2003).
- Dutta, U., Chatterjee, P., Roca i Cabarrocas, P., Chaudhuri, P. & Vanderhaghen, R. Calculation of the position-dependent inner collection efficiency in PIN solar cells using an electrical-optical model. *J. Non-Cryst. Solids* **338–340**, 677–681 (2004).
- Guha, S. *et al.* Band-gap profiling for improving the efficiency of amorphous silicon alloy solar cells. *Appl. Phys. Lett.* **54**, 2330–2332 (1989).
- Faughnan, B. W. & Crandall, R. S. Determination of carrier collection length and prediction of fill factor in amorphous silicon solar cells. *Appl. Phys. Lett.* **44**, 537–539 (1984).
- Hack, M. & Shur, M. Physics of amorphous silicon alloy p-i-n solar cells. *J. Appl. Phys.* **58**, 997–1020 (1985).
- Massiot, I. *et al.* Multi-resonant absorption in ultra-thin silicon solar cells with metallic nanowires. *Opt. Express* **21**, A372–A381 (2013).

## Acknowledgments

This research was supported by Korea Research Council of Fundamental Science and Technology (KRCF) and Korea Institute of Science and Technology (KIST) for National



Agenda Project (NAP) program and Project No. 2E24821. Also, it was supported by the Global Frontier R&D Program on Center for Multiscale Energy System funded by the National Research Foundation under the Ministry of Science, ICT & Future Planning, Korea (Grant Nos. 2011-0031561 and 2012M3A6A7054856). D.-K.L. acknowledges the support by a grant for the KUUC program.

### Author contributions

D.-K.L., S.H. and J.Y. designed the project and supervised the entire experimental and simulation processes. T.K., H.K., J.P., H.K., Y.Y., S.-M.K., C.S. and H.J. performed all experiments and calculations. I.K., D.S.J. and C.K. discussed the simulation results. H.K., J.Y.K., B.K., M.J.K. and H.J.S. helped experimental data analysis. The manuscript was primarily written by T.K. and revised by D.-K.L.

### Additional information

**Supplementary information** accompanies this paper at <http://www.nature.com/scientificreports>

**Competing financial interests:** The authors declare no competing financial interests.

**How to cite this article:** Kim, T. *et al.* Triple-Junction Hybrid Tandem Solar Cells with Amorphous Silicon and Polymer-Fullerene Blends. *Sci. Rep.* 4, 7154; DOI:10.1038/srep07154 (2014).



This work is licensed under a Creative Commons Attribution-NonCommercial-ShareAlike 4.0 International License. The images or other third party material in this article are included in the article's Creative Commons license, unless indicated otherwise in the credit line; if the material is not included under the Creative Commons license, users will need to obtain permission from the license holder in order to reproduce the material. To view a copy of this license, visit <http://creativecommons.org/licenses/by-nc-sa/4.0/>